# Thermal Analysis of Yttrium and Cerium Based Nanostructured Powders for High Temperature Applications

Madhusudhana R[1], R. Gopalakrishne Urs[2], L. Krishnamurthy[3]
[1]*Department of Physics, The National Institute of Engineering, Mysuru-08, India*
[2]*Department of Mechanical Engineering, The National Institute of Engineering, Mysuru-08, India*

***Abstract*** **- As they deal with extremely high temperature, corrosive, and oxidative environments, Thermal Barrier Coatings (TBCs) are one of the key types of coating that demonstrates the promising features for aerospace applications. Since they exhibit exceptional qualities such a high surface to volume ratio, melting point, and thermal characteristics due to their nano-sized structural behaviour when compared to traditional TBCs, nanostructured thermal barrier coatings (N-TBCs) are also commonly used in aerospace applications. The synthesis and characterisation of yttrium nanopowders, cerium nanopowders, and cerium and yttrium doped TiO2 nanopowders produced utilising the sol-gel wet chemical synthesis method are the main goals of this work. Researchers looked at the surface morphology, chemical makeup, crystalline behaviour, and thermal behaviour of the produced powders. and analyzed by performing SEM (Scanning Electron Microscope), EDX (Energy Dispersive X-ray Analysis), XRD (X-Ray Diffractometer) and TGA (Thermo-Gravimetric Analysis) analysis techniques.**

***Index Terms*** **- TBCs, N-TBCs, XRD, SEM, EDX and TGA.**

## 1.INTRODUCTION

As they deal with extremely high temperature, corrosive, and oxidative environments, Thermal Barrier Coatings (TBCs) are one of the key types of coating that demonstrates the promising features for aerospace applications. For a TBC to function effectively under demanding thermo-mechanical conditions, it must adhere to a number of specifications. Sufficient porosity is needed to regulate warm extension strains during warming and cooling, as well as proper warm development coefficient cooperation with the metal surface that the TBC is covering. Stage security is necessary to prevent the massive volume changes that occur during stage changes from causing the covering to spall or shatter. Resistance to oxidation, as well as respectable mechanical qualities for pivoting/moving parts or parts in contact, are essential in air-breathing motors. As a result, the general requirements for an effective TBC can be summed up as follows: a high melting point is one. 2) There is no phase transition between working temperature and room temperature. three) A low heat conductivity. 4) Lack of chemical action. 5. Equivalent warm extension match with metallic substrate. 6) Outstanding substrate adhesion. 7) a permeable microstructure with a low sintering rate. The number of materials that can be used is severely constrained by these requirements, with ceramic materials typically having the option to possess the required qualities.

Four layers are typically present in thermal barrier coatings: a metallic bond coat, a ceramic top coat, a metal substrate, and a thermally generated oxide (TGO). Yttria-stabilized zirconia (YSZ), which has an exceptionally low conductivity and is stable at the elevated operating temperatures frequently encountered in TBC applications, is typically used as the ceramic coating. The TBC's largest warm angle is created by the ceramic layer, which also helps to keep the bottom layers cooler than the surface. YSZ has abrupt stage transitions over 1200°C, going from t'-tetragonal to tetragonal, tetragonal to cubic, and cubic to monoclinic. Such stage changes cause cracks to form inside the top coat. Recent studies comparing ceramic topcoats to several innovative ceramic materials (such as zirconates) have found that they perform best at temperatures beyond 1200°C but are less durable and tough than YSZ. Additionally, these zirconates may have a high concentration of oxygen-

particles, which could enhance the formation of the TGO by assisting oxygen diffusion. The coating may spallate with a thick enough TGO, which is undesirable for TBCs.

The term "nano-coating" refers to the surface-designing process that uses atomistic or subatomic statements in thin, under 100 nm, layers. As a result, the thickness of the nano-coating layers produced by these cycles differs significantly from the bulk coating development processes, such as electroless plating, electroplating, plasma enhanced chemical vapour deposition (PE-CVD), physical vapour deposition, and laser vaporisation. Based on the conditions under which they operate, PVD is typically grouped with other vacuum processes including ion plating, sputtering, and ion-beam aided deposition. The process of depositing ions, molecules, or atoms from the precursor material to be deposited after decomposition is known as chemical vapour deposition (CVD). Additionally, various effective chemical processes are used to create nano-structured coatings, including chemical bath deposition, sol-gel, emulsion, solvo-thermal, hydrothermal, and electrochemical processes. These coatings are so popular because of their distinctive and appealing characteristics, such as their high surface-to-volume ratio and a variety of additional electrical, chemical, mechanical, physical, optical, thermal, and magnetic capabilities than TBCs because of their nano-regime. Thus, TBCs are being replaced by N-TBCs as a result of these distinctive features. These nano-structured thermal barrier coatings (N-TBCs) are used extensively in aerospace applications because they exhibit exceptional qualities, such as a high surface-to-volume ratio, melting point, phase stability, and thermal stability, which are caused by the structural behaviour of nanoscale materials as opposed to bulk materials or traditional TBCs. Since yttrium, zirconium, and cerium have high melting points, excellent phase stability, and low thermal conductivity properties, these materials are typically used to make TBCs. So, in our current investigation, the identical yttrium and cerium material composition has been used. In addition to the aforementioned thermodynamic behaviours, yttrium and cerium are undoubtedly compatible to use in TBCs or N-TBCs; therefore, to obtain the improved and enhanced thermal stability and phase stability properties desired for TBCs applications, these powders were doped to prepare TiO2 powder since it has a high melting point of approximately 1843 oC.

Sol-gel wet chemical synthesis was used to create the TiO2, cerium doped TiO2, and yttrium and cerium doped TiO2. This sol-gel approach is used because it gives great coating morphological homogeneity, coating purity, and a range of coating thicknesses depending on the calcination temperature we take into account. Highly adherent nano-structured coatings are generated by using sol-gel coatings. Additionally, phase stability and its fluctuations are influenced by the coatings' % material composition. SEM (Scanning Electron Microscope), EDAX (Energy Dispersive X-ray Analysis), XRD (X-Ray Diffractometer), and TGA (Thermo-Gravimetric Analysis) were used to characterise the synthesised nanopowders in order to determine their surface morphology, chemical composition, crystallinity behaviour, and thermal stability.

## 2.EXPERIMENTAL DETAILS

### 2.1 MATERIALS AND METHOD

Titanium (IV) isopropoxide, ethanol, cerium (III) nitrate hexahydrate, yttrium (III) nitrate hexahydrate were materials used in our present work. The sol-gel chemical synthesis technique has been implemented in this study to synthesize $TiO_2$ nanopowder, cerium doped $TiO_2$ nanopowder and yttrium and cerium doped $TiO_2$ nanopowder.

### 2.2 SYNTHESIS PROCEDURE

#### 2.2.1 SYNTHESIS OF $TIO_2$ NANO-POWDER

Initial experiments involved dissolving 5 grammes or 5 ml of titanium tetra (IV) isopropoxide (figure 1) in 35 ml of ethanol solution, which was then swirled continuously for an hour at a speed of 360 rpm and at a temperature of 40 °C using a magnetic stirrer. 9ml of distilled water was added for the same solution after an hour. After adding distilled water, the solution combination was heated for 180 minutes while being swirled and heated using a magnetic stirrer, as illustrated in figure 2, to maintain a temperature of around 40°C. The identical solution reached a white colour semi-liquid state after 180 minutes, and this was then calcined at a temperature of 300°C to produce white colour TiO2 nano powder. (figure 5).



Figure 1: Yttrium precursor used for synthesis procedure Figure 2: $TiO_2$ solution under stirring

2.2.2 SYNTHESIS OF CERIUM DOPED $TIO_2$ NANO-POWDER

Additionally, a magnetic stirrer was used to stir and heat a solution of 6ml or 6 grammes of titanium (IV) isopropoxide and 42ml of ethanol continuously for an hour at a temperature of 50°C and a rotational speed of 770–780 rpm. At a temperature of 65°C, agitate the entire solution while adding 10ml of distilled water dropwise after one hour. Using a magnetic stirrer, 0.18g of cerium (III) nitrate hexahydrate was added to the solution after 5 minutes. Additionally, as depicted in figure 3, a magnetic stirrer was used to continuously heat and stir the solution combination at a temperature of 65 °C while rotating at 750 rpm. Once more, add 10ml of distilled water dropwise to the solution and stir with a magnetic stirrer rotating at 1000 rpm for 30 minutes at room temperature. After 30 minutes, the solution mixture reached a semi-liquid state. After calcining the semi-liquid condition of solution (figure 4) for around three hours at a temperature of 300°C, a pale yellowish powder (figure 6) of 3% cerium doped TiO2 was eventually produced.


Figure 3: Y-$TiO_2$ solution under stirring Figure 4: Y-$TiO_2$ precipitate

2.2.3 SYNTHESIS OF CERIUM AND YTTRIUM DOPED $TIO_2$ NANO-POWDER

At first, a solution of 6g or 6ml of titanium (IV) isopropoxide and 42ml of ethanol was swirled and heated continuously for an hour at a temperature of 50°C with a rotating speed of 310-320rpm. Using a magnetic stirrer, 10ml of distilled water was added dropwise after one hour and heated and swirled again at a constant temperature of 40°C. After 5 minutes, 0.9 grammes of cerium (III) nitrate hexahydrate and 0.9 grammes of yttrium (III) nitrate hexahydrate were combined and heated at 40 °C for 10 minutes while being stirred with a magnetic stirrer rotating at 750 rpm. After 5 minutes, 10 ml of distilled water was added dropwise, and the mixture was stirred with a magnetic stirrer at 300 rpm for 150 minutes at room temperature. Finally, the obtained semi-liquid solution combination was allowed to undergo the calcination operation at the temperature of 480°C for the period of 210min to generate yellowish 3% yttrium-cerium doped TiO2 powder (figure 7).

Figure 5: Synthesized $TiO_2$ powder Figure 6: Synthesized Y-$TiO_2$ powder

Figure 7: Synthesized Y/Ce-$TiO_2$ powder

2.3 CHARACTERIZATION

2.3.1 ANALYSIS ON SURFACE MORPHOLOGY

A type of electron magnifying device called a scanning electron microscope (SEM) creates images of the material by analysing the surface with activated light emission. The electrons interact with the molecules in the sample and produce a variety of

signals that provide information about the sample's surface and composition. The beam position is combined with the strength of the recognised sign to convey an image, and the electron shaft is inspected using a raster check design. Typically, auxiliary ions that were emitted from component parts exposed to the negative ions shaft and detected using an optional negative ion recognizer were commonly recognised in various scanning routes. Sample materials can be observed in high vacuum in a standard SEM, low vacuum or wet conditions in a variable pressure or SEM environment, and at a variety of cryogenic or elevated temperatures using specific equipment. The high magnification SEM picture of synthetic TiO2 nanopowder shown in figure 8 illustrates the existence of irregularly scattered TiO2 nanoparticles. Figure 9 shows a low-magnification SEM image of synthetic TiO2 nanopowders, showing the significant degree of agglomeration of nanoparticles as well as the uneven distribution of nanoparticles.

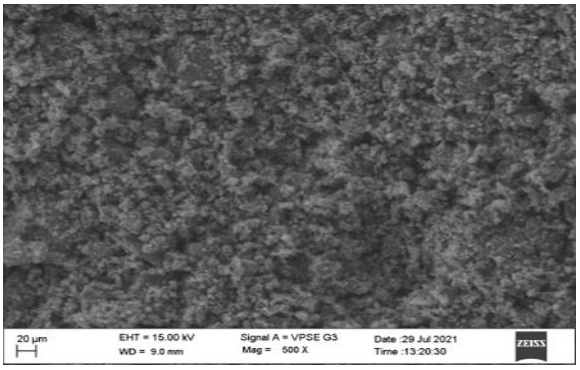


Figure 8: Low magnified SEM image of $TiO_2$ powder
Figure 9: High magnified SEM image of $TiO_2$ powder
Figure 10 is also a low magnified SEM image of developed $TiO_2$ nano powder, that reveals the average particle size of about 158.4nm.

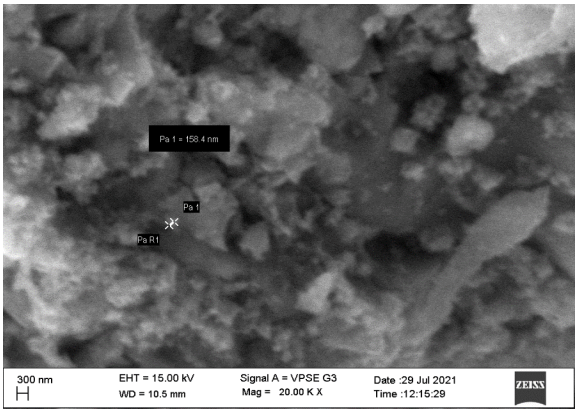


Figure 10: High magnified SEM image $TiO_2$ nano powder

Figure 11 shows the well-defined structure and enhanced surface morphological features of produced Ce doped TiO2 nanoparticles in a high magnification SEM picture of Cerium doped TiO2 nanopowder. Figure 12 is a highly magnified SEM image that shows a significant buildup of nanoparticles as well as the non-homogeneity of their distribution.

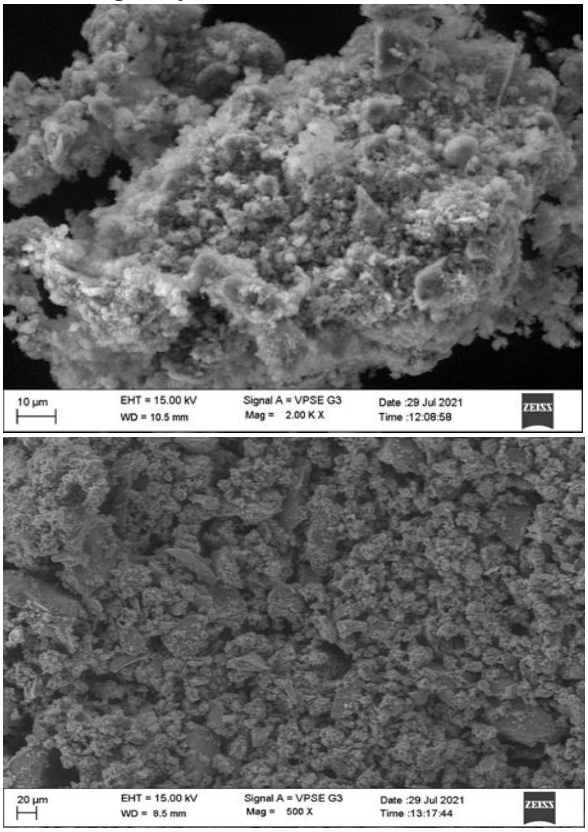


Figure 11: Low magnified SEM image Ce doped $TiO_2$ nano powder

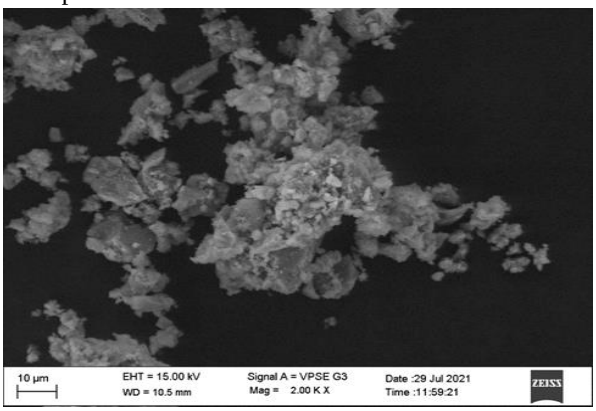


Figure 12: High magnified SEM image Ce doped $TiO_2$ nano powder

Figure 13 is also the high magnified SEM image of developed Cerium doped $TiO_2$ nano powder, which represents the average particle size of about 147.2nm.

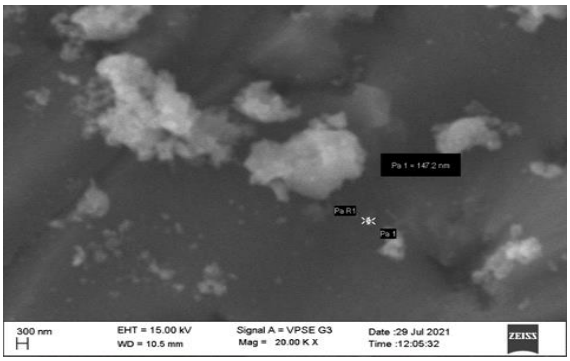


Figure 13: High magnified SEM image of Ce doped$TiO_2$ powder

The low-magnified SEM picture of synthetic Yttrium and Cerium doped TiO2 nano powder is shown in Figure 14. Compared to previously manufactured, undoped nano powders, it shows highly defined, larger-sized nano particles with just a little aggregation. A high magnification SEM image of the generated Yttrium and Cerium doped TiO2 nano powder in figure 15 further confirms the presence of aggregated nanoparticles. Figure 16 depicts a SEM picture of generated Cerium doped TiO2 nanopowder with a high magnification and an average particle size of 170.8 nm.

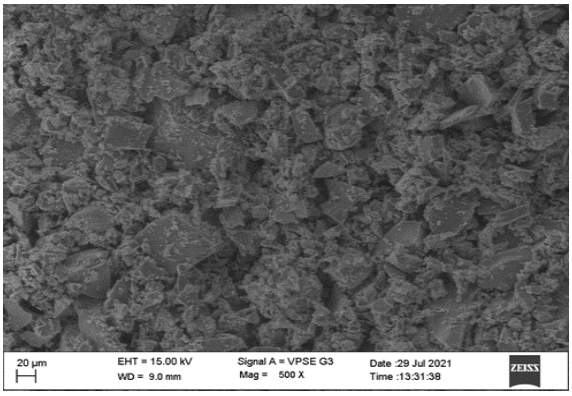


Figure 14: Low magnified SEM image of Y/Ce doped$TiO_2$ powder

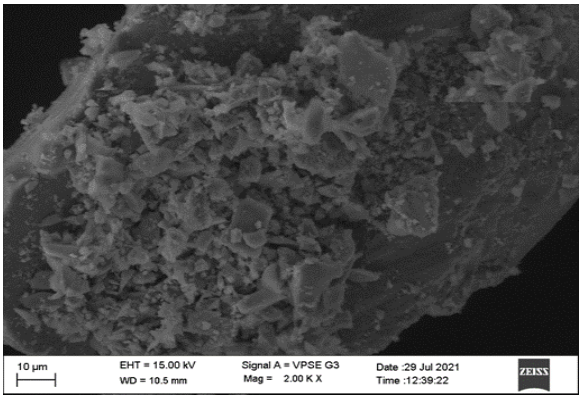


Figure 15: High magnified SEM image of Y/Ce doped$TiO_2$ powder

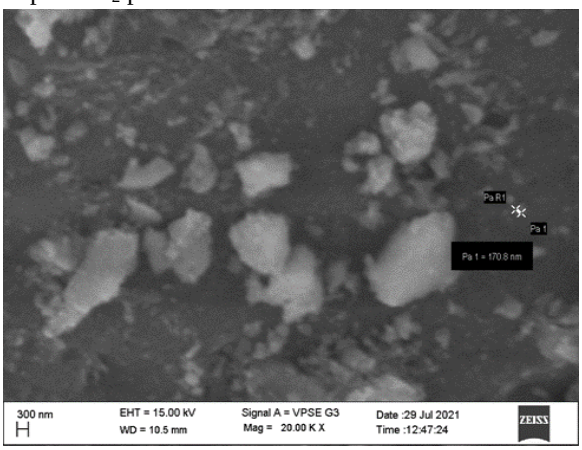


Figure 16: High magnified SEM image of Y/Ce doped$TiO_2$ powder

The bear TiO2 powder's average particle size was found to be 158.4 nm. However, the average particle size was reduced to 147.2 nm when cerium alone was added to TiO2 powder. This occurred because Ce ions were now present in the lattice point. The average particle size was observed to grow by 170.8 nm as the number of dopants was increased from cerium to cerium and yttrium. This was due to enhanced lattice characteristics brought on by the presence of both Ce and Y ions.

### 2.3.2 ANALYSIS ON CHEMICAL/ELEMENTAL COMPOSITION

Energy-dispersive X-beam spectroscopy, sometimes referred to as energy dispersive X-track microanalysis (EDXMA), energy dispersive X-track inquiry (EDAX or EDXA), or simply EDX, is a methodological technique used for the fundamental analysis or compound representation of the material. It depends on the sample's relationship with an X-ray excitation source. Its ability to portray things is mostly due to its prominent location, since each module has a unique individual and modest construction allowance as well as an amazing system of peaks on its EM outflow broadband. The Moseley's law predicts peak positions with an accuracy significantly greater than the trial aim of a typical EDX instrument.

Figure 17 is an EDX image of synthetic TiO2 nanopowder that shows significant titanium and oxygen traces with weight percentages of 59.0% and 38.2% and nitrogen traces with weight percentage of 2.9%.

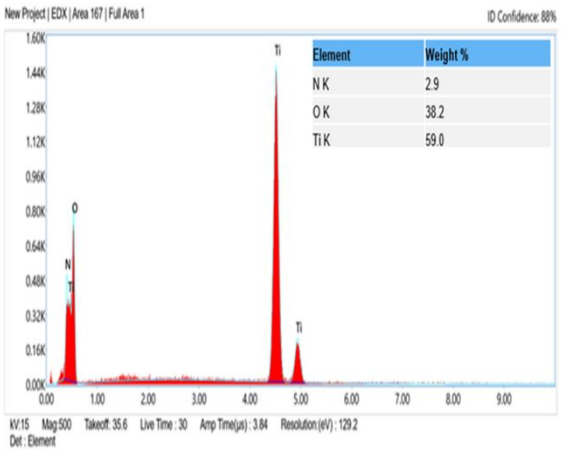


Figure 17: EDX image of $TiO_2$ powder

The EDX picture of produced Cerium-doped TiO2 nanopowder is shown in Figure 18. The graph below demonstrates the significant amounts of titanium and oxygen (60.0% and 34.7% of the total weight, respectively), and it also confirms the existence of doped cerium (5.3% of the total weight).

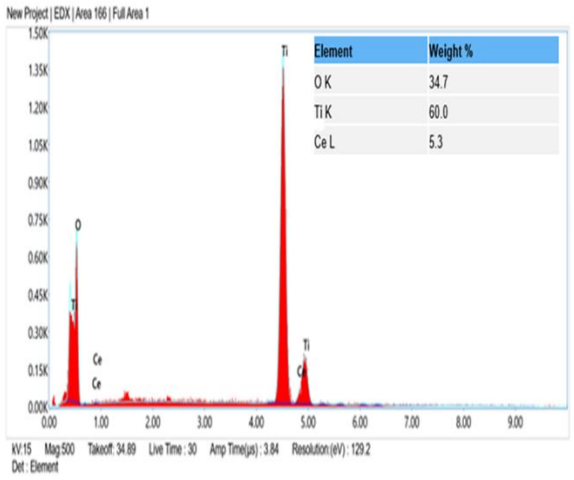


Figure 18: EDX image of Ce doped $TiO_2$ powder

Figure 19 represents EDX image of synthesized Yttrium and Cerium doped $TiO_2$ nano powder depicting the large amount of traces of titanium and oxygen with 48.8% and 30.4% weight percentages along with the small traces of carbon and bromine with 3.0% and 1.5% weight percentages. The image also assures the presence of added yttrium and cerium with 3.8% and 12.6 weight percentages respectively.

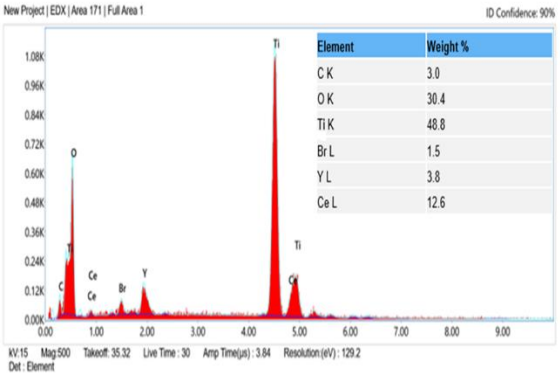


Figure 19: EDX image of Y/Ce doped $TiO_2$ powder

2.3.3 XRD (X-RAY DIFFRACTOMETER) ANALYSIS

The exploratory science known as the X-ray diffractometer (XRD) determines a sample's nuclear and subatomic structure by using light-emitting X-rays that diffract into a variety of distinct patterns due to the translucent design. The thickness of the electron layer within the sample can be visualised in three dimensions by a crystallographer by measuring the positions and forces of these diffracted radiates. The mean locations of the molecules in the crystal sample, as well as their crystallographic problem, compound bonds, and various other information, can be determined from this electron thickness.

An XRD picture of synthetic TiO2 nanopowder is shown in Figure 20. The image shows the powerful peak, which has an intensity value of around 228.19 at 25.41 2. Smaller peaks at 2 values of roughly 38.04, 48.16, 54.69, and 62.87 are connected to the outcome. The image also revealed that the powder had an 88.46% crystallinity and an 11.54% amorphous nature, with the TiO2 nanopowder specifically being polycrystalline in nature. And 6.61 nm was determined to be the average particle size value.

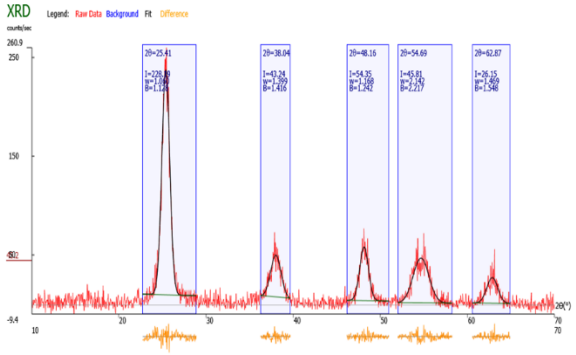


Figure 20: XRD image of $TiO_2$ powder

| Peak | 2 K1 | dcalc (Å) | Height (cps) | Relative Height | Integral Intensity | Eqn | Summed Intensity | FWHM | Integral Breadth | Asymmetry |
|---|---|---|---|---|---|---|---|---|---|---|
| 1 | 25.4098 | 3.50247 | 228.2 | 999 | 257.50 | G | 257.21 | 1.0601 | 1.1284 | 1.0000 |
| 2 | 38.0376 | 2.36376 | 43.2 | 189 | 61.23 | G | 61.29 | 1.3989 | 1.4162 | 1.0000 |
| 3 | 48.1607 | 1.88790 | 54.3 | 238 | 67.50 | G | 67.98 | 1.1677 | 1.2420 | 1.0000 |
| 4 | 54.6904 | 1.67693 | 45.8 | 201 | 101.54 | G | 102.44 | 2.1424 | 2.2166 | 1.0000 |
| 5 | 62.8666 | 1.47706 | 26.1 | 114 | 40.47 | G | 41.33 | 1.4691 | 1.5479 | 1.0000 |

Table 1: XRD data of $TiO_2$ powder

An XRD picture of synthetic Cerium-doped TiO2 nanopowder is shown in Figure 21. The figure showed a high intensity peak with an intensity value of roughly 3350 at a value of 27.0459 2. The corresponding minor peaks, which appeared at smaller intensities between 30 and 40, 40 to 50, 50 to 60, at 70, and between 70 and 80, were depicted by the figure. Furthermore, it showed that the powder had less crystallinity. And 8.01nm was determined to be the average crystallite size value.

Figure 21: XRD image of Ce doped $TiO_2$ powder

| Peak | 2-theta (deg) | D (ang.) | Height (counts) | FWHM (deg) | Int. I (counts deg) | Int. W (deg) | Asym. factor | eta L/mL | eta H/mH | Size (ang.) | Rel. int. I | Rel. height | Peak shape |
|---|---|---|---|---|---|---|---|---|---|---|---|---|---|
| 1 | 25.4204 | 3.50102 | 107.25 | 0.9536 | 143.15 | 1.3347 | 0.9768 | 0.7923 | 0.6924 | 89.2 | 100 | 100 | Split pseudo-Voigt |
| 2 | 48.1188 | 1.88945 | 25.25 | 1.2055 | 32.41 | 1.2833 | 1.0616 | 0.0001 | 0.0002 | 75.38 | 22.64 | 23.55 | Split pseudo-Voigt |
| 3 | 62.6647 | 1.48133 | 12.65 | 1.2807 | 19.01 | 1.5035 | 0.7764 | 0 | 0.4793 | 75.85 | 13.28 | 11.79 | Split pseudo-Voigt |

Table 2: XRD data of Ce-$TiO_2$ powder

An XRD picture of produced Yttrium and Cerium doped TiO2 nano powder is shown in Figure 22. The outcome showed the existence of smaller peaks with values ranging from 20 to 30 2, as well as much smaller peaks with extremely low intensities. When Yttrium and Cerium were added to TiO2 nanopowder, the crystal structure was reduced. And 4.06 nm was determined to be the average particle size value.

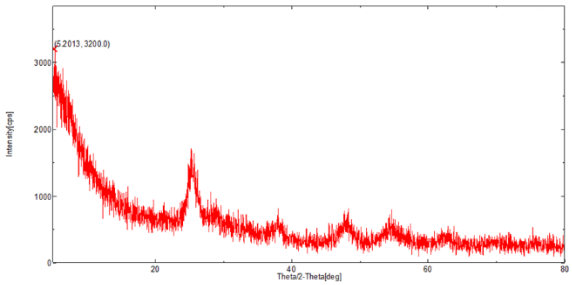


Figure 22: XRD image of Ce/Y doped $TiO_2$ powder

| Peak | 2-theta (deg) | D (ang.) | Height (counts) | FWHM (deg) | Int. I (counts deg) | Int. W (deg) | Asym. factor | eta L/mL | eta H/mH | Size (ang.) | Rel. int. I | Rel. height | Peak shape |
|---|---|---|---|---|---|---|---|---|---|---|---|---|---|
| 1 | 25.4204 | 3.50102 | 107.25 | 0.9536 | 143.15 | 1.3347 | 0.9768 | 0.7923 | 0.6924 | 89.2 | 100 | 100 | Split pseudo-Voigt |
| 2 | 48.1188 | 1.88945 | 25.25 | 1.2055 | 32.41 | 1.2833 | 1.0616 | 0.0001 | 0.0002 | 75.38 | 22.64 | 23.55 | Split pseudo-Voigt |

| | | | | | | | | | | | | | |
|---|---|---|---|---|---|---|---|---|---|---|---|---|---|
| 3 | 62.6647 | 1.4813 3 | 12.65 | 1.2807 | 19.01 | 1.503 5 | 0.776 4 | 0 | 0.479 3 | 75.85 | 13.2 8 | 11.7 9 | Split pseudo -Voigt |

Table 3: XRD data of Ce/Y-$TiO_2$ powder

Due to the different atom sizes of cerium and yttrium compared to TiO2 atoms, it was discovered that the XRD peaks of Ce doped and Y/Ce doped TiO2 powders were displaced. When compared to the host TiO2 powder, the peaks here after doping widen.

2.3.4 ANALYSIS ON THERMAL STABILITY

Thermo-gravimetric analysis (TGA), also known as thermo-gravimetric investigation, is a technique for thermal examination that estimates the mass of the sample over time as the temperature varies. This estimation provides information on both chemical and physical phenomena, such as stage shifts, ingestion, adsorption, and desorption.

The thermo-gravimetric analysis (TGA) of TiO2 powder is depicted in Figure 23 and displays the type 2 TG (thermo-gravimetric) curve. As a result of an increase in temperature, Type 2 curves show desorption nature or dryness in the material composition. Furthermore, the TiO2 powder was only thermally stable up to 101.9°C, and as the temperature rose, it began to break down. This was indicated by the onset value of around 101.9°C. The TGA analysis offers information about DTA in addition to TG curves (differential thermal analysis). At temperatures between 99.4°C and 148.5°C, the TiO2 powder displayed exothermic reaction, according to DTA.

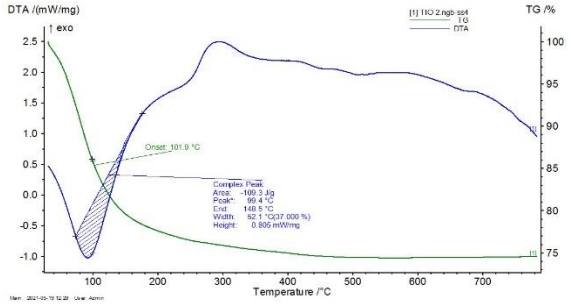


Figure 23: TGA image of $TiO_2$ powder

The TGA analysis result of Ce-doped TiO2 powder is shown in Figure 24. The graphic shows that Ce-TiO2 powder displays type 1 form of TG curve, explaining that there is no change in the material composition or loss in the material composition as its onset value was approximately 755.6°C, making Ce-TiO2 more thermally stable than the other two powders. When temperatures between 408.9°C and 478.3°C were reached, Ce-TiO2 was exothermic, according to the DTA data.

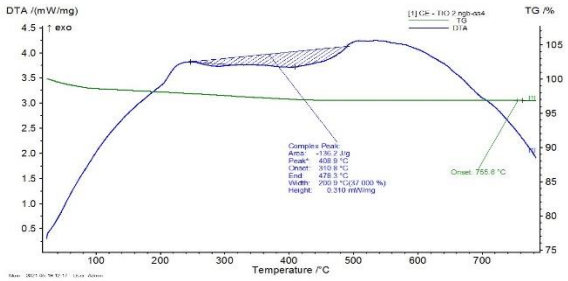


Figure 24: TGA image of Cerium doped $TiO_2$ powder

The TGA result of Y/Ce-TiO2 powder is shown in Figure 25. The outcome shows that Y/Ce-TiO2 powder exhibits type 2 TG curve, which means that when temperature rises, the material composition either experiences desorption or dryness. The material was more thermally stable than TiO2 powder, as evidenced by the onset value of approximately 347.0°C. Additionally, the DTA results demonstrated that the Y/Ce-TiO2 powder was exothermic from 417.2°C to 457.2°C.

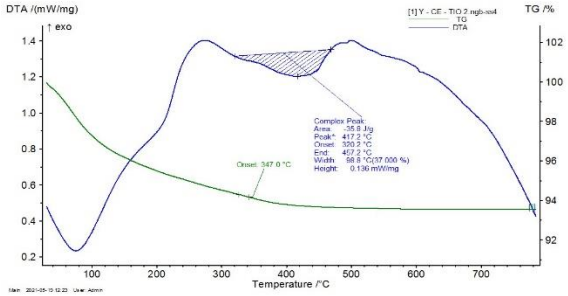


Figure 25: TGA image of Y/Ce doped $TiO_2$ powder

RESULTS AND DISCUSSION

The task was completed by employing the sol-gel method to create titanium dioxide powder using titanium tetra-iso propoxide as a precursor material. Cerium doped TiO2 and yttrium-cerium doped TiO2, as well as cerium(III) nitrate hexahydrate and yttrium(III) nitrate hexahydrate, were both produced using the same precursor. The considerable quantity of agglomeration and uneven distribution of nanoparticles associated with the average nanoparticle

size of around 158.4nm were visible in low-magnification SEM images of synthetic TiO2 nanopowder. The non-uniform distribution of nanoparticles was also visible in the high magnification SEM image of TiO2 nanopowder. When compared to TiO2 nanoparticles, the high and low magnification SEM images of Cerium doped TiO2 nanopowder showed a non-homogeneous dispersion of nanoparticles with somewhat distinct structures. And it was discovered that the doped TiO2 nanopowder had an average particle size of 147.2 nm. When compared to TiO2 and cerium doped TiO2 nano powders, SEM pictures of yttrium and cerium doped TiO2 nano powder also showed a minor aggregation in the particle composition with clearly defined structures. And The observed average particle size was 170.8 nm. Changes in lattice parameters were also seen to affect particle size. With weight percentages of 59.0% and 38.3% for TiO2, 60.0% and 34.7% for cerium doped TiO2, and 48.8% and 30.4% for yttrium and cerium doped TiO2, respectively, EDX results showed the variable percentage composition of titanium and oxygen. Additionally, it was found that cerium doped TiO2 had a cerium composition of 5.3% weight percentage, while yttrium and cerium doped TiO2 had cerium and yttrium compositions of roughly 12.6% and 3.8% weight percentages, respectively.

The crystalline nature was seen to decrease as the doping condition or the doping material was increased, according to the XRD results. Comparing the TiO2 nanopowder to cerium doped TiO2 and yttrium and cerium doped TiO2 nanopowders, we found that the TiO2 nanopowder was highly crystalline in nature. Additionally, the TiO2 powder's XRD results revealed that it is polycrystalline in nature due to the emergence of peaks at 2 values of 25.41, 38.04, 48.16, 54.69, and 62.87.

The results of the thermo-gravimetric analysis (TGA) showed that the onset temperature of TiO2 powder was 101.9°C, the onset temperature of Ce/TiO2 was 755.6°C, and the onset temperature of Y/Ce/TiO2 was 347.0°C. This showed that Ce/TiO2 was much more thermally stable than Y/Ce/TiO2 and that Y/Ce/TiO2 was also more thermally The results revealed that, $Ce/TiO_2$ was much thermally stable than bare $TiO_2$ powder and $Y/Ce/TiO_2$ powder.

## CONCLUSION

The most promising technique for creating nanostructured coatings is sol-gel wet chemical synthesis. The combination of yttrium and cerium offers high melting point, low thermal conductivity, and consistent phase stability. Sol-gel synthesis was used in the current study to create TiO2 nanopowder, Cerium doped nanopowder, and Cerium and Yttrium doped nanopowders. The information about particle size and agglomeration was disclosed by the SEM picture results. Changes in lattice parameters were also seen to affect particle size. After doping that specific material in the TiO2 powder, EDX results showed the traces of the appropriate material composition, which were obvious for the presence of cerium and yttrium. The XRD results demonstrated the polycrystalline character of TiO2 nanopowder and revealed that the crystalline nature decreased with increasing doping. According to TGA studies, cerium doped TiO2 nanopowder was much more thermally stable than other TiO2 nanopowders and Yttrium and Cerium doped TiO2 nanopowder. Therefore, it is possible to use these nanopowders in TBC applications by taking into account their primary attribute of temperature stability. To meet the requirements for creating extremely resilient nano-structured thermal barrier coatings, these powders can also be employed to create the relevant coatings. Their structural and thermal properties can then be studied and compared with the results from above (N-TBCs).

## REFERENCE

[1] Daniel W Parker, Materials and Design 1992 VoI. 13 No. 6

[2] R.A.Miller, 1997 Journal of Thermal Spray Technology,Volume6(1)March

[3] S. Yasodhai, T. Sivakumar, S. Govindarajan, 1999 Thermochimica Acta 338 57±65

[4] Antonino Gulinoa, Giuseppe Compagnini, Russell G. Egdell, Ignazio Fragala Á, Thin Solid Films 352 73±76

[5] J.A. Nesbitt, 2000 Surface and Coatings Technology 130 141-151

[6] Uwe Schulz, Christoph Leyens, Klaus Fritscher, Manfred Peters, Bilge Saruhan-Brings, Odile Lavigne, JeanMarc Dorvaux, Martine Poulain, Remy Mévrel, Michaël Caliez, 2003 Aerospace Science and Technology 7 73–80

[7] Kazuhide Matsumoto, Yoshiyasu Itoh, Tsuneji Kameda, 2003 Science and Technology of Advanced Materials 4 153–158
[8] H. K. Sezer, A. J. Pinkerton, Lin Li, and P. Byrd, 2005 Journal of Laser Applications 17, 225
[9] Thierry Grosdidier, Gang Ji, Nathalie Bozzolo, 2006 Intermetallics 14(7), 715-721
[10] Ravinder Kaur, AV Singh, Kiran Sehrawat, NC Mehra, RM Mehra, 2006 Journal of non-crystalline solids 352(23-25) 2565-2568
[11] Xianliang JIANG, Chunbo LIU and Feng LIN, 2007 J. Mater. Sci. Technol., Vol.23 No.4
[12] Gabriel Maria Ingo, Tilde de Caro, Acta Materialia, 2008 56 5177–5187
[13] Baomei Wen, Yizhong Huang, John J Boland, 2008 The Journal of Physical Chemistry C 112(1) 106-111
[14] Qiang Zhang, Chang-Jiu Li, Yong Li, Shao-Ling Zhang, Xiu-Ru Wang, Guan-Jun Yang, and Cheng-Xin Li, 2008 Journal of Thermal Spray Technology Vol 17(5-6)
[15] F Rovere, PH Mayrhofer, A Reinholdt, J Mayer, JM Schneider, 2008 Surface and Coatings Technology 202(24) 5870-5875
[16] C.K. Chung, Y.L. Chang and T.S. Chen, 2009 978-1-4244-4630-8/09/$25.00 ©2009 IEEE
[17] D. D. Hass and H. N. G. Wadley, 2009 J. Vac. Sci. Technol. A 272
[18] LIU Chun-bo, ZHANG Zhi-min, JIANG Xian-liang, LIU Min, 2009 Trans. Nonferrous Met. Soc. China 19 99í107
[19] Xiaolong Chen, Yanfei Zhang, Xinhua Zhong, Zhenhua Xu, Jiangfeng Zhang, Yongliang Cheng, Yu Zhao, Yangjia Liu, Xizhi Fan, Ying Wang, Hongmei Ma, Xueqiang Cao, 2010 Journal of the European Ceramic Society 30 1649–1657
[20] E.P. Busso, H.E. Evans b, Z.Q. Qian C, M.P. Taylor, 2010 Acta Materialia 58 1242– 1251
[21] F Rovere, D Music, JM Schneider, PH Mayrhofer, 2010 Acta materialia 58(7) 2708-2715
[22] D. D. Hass Æ Y. Y. Yang Æ H. N. G. Wadley, 2010 J Porous Mater 17:27–38
[23] SUN Jie, ZHANG Lili, ZHAO Dan, 2010 JOURNAL OF RARE EARTHS, Vol. 28, Spec. Issue, p. 198
[24] Matthew R. Begley and Haydn N.G. Wadley, 2011 The American Ceramic Society [S1] S96–S103
[25] Sorina ILINA, Gheorghe IONESCU, Victor MANOLIU, Radu Robert PITICESCU, 2011 INCAS BULLETIN, Volume 3, Issue 3
[26] Zhuo Yu, Hengbei Zhao, and Haydn N. G. Wadley, 2011 Journal of the American Ceramic Society Vol. 94, No. 8
[27] Cody H. Nguyena, K. Chandrashekhara b, Victor Birman, 2012 Mechanics Research Communications 39 35–43
[28] Madhusudhana R, Lovesome Benedict S, Sushma S, L Krishnamurthy, R Gopalkrishne Urs, Sachin D, 2020 Shodh Sarita Vol.7, Issue 27(III)